Available online at www.sciencedirect.com
SCIENCE DIRECT®
Journal of Catalysis 232 (2005) 85–95
JOURNAL OF CATALYSIS
www.elsevier.com/locate/jcat

In situ UV–vis studies of the effect of particle size on the epoxidation of ethylene and propylene on supported silver catalysts with molecular oxygen

Jiqing Lu [a], Juan J. Bravo-Suárez [a], Atsushi Takahashi [a], Masatake Haruta [b], S. Ted Oyama [a,c,*]

[a] *Research Institute for Innovation in Sustainable Chemistry, National Institute of Advanced Industrial Science and Technology, AIST Tsukuba West, 16-1 Onogawa, Tsukuba, Ibaraki 305-8569, Japan*
[b] *Department of Evaluation, National Institute of Advanced Industrial Science and Technology, AIST Tsukuba Central 2nd, 1-1-1 Umezono, Tsukuba, Ibaraki 305-8568, Japan*
[c] *Environmental Catalysis and Nanomaterials Laboratory, Department of Chemical Engineering (0211), Virginia Polytechnic Institute and State University, Blacksburg, VA 24061, USA*

Received 3 December 2004; revised 9 February 2005; accepted 15 February 2005

Available online 7 April 2005

Abstract

In this study the effect of particle size on ethylene and propylene epoxidation was studied on a series of silver catalysts supported on $CaCO_3$ with loading levels of 0.5–56 wt%. Particle sizes determined from O_2 chemisorption uptakes at 443 K (170 °C) ranged from 50 to 660 nm, and this was confirmed by field emission scanning electron microscopy, which in addition showed crystallite agglomeration at high loadings. Reaction results show that large particles favor ethylene epoxidation by 3–5-fold at 473–493 K, whereas particle size does not have a large effect on propylene epoxidation. X-Ray diffraction measurements indicate that the bulk of the particles consist of silver in a metallic state, but in situ ultraviolet–visible (UV–vis) spectroscopy distinctly shows that in addition to a metallic component, small particles have silver in Ag^+ state. The small particles are probably covered by a layer of Ag_2O, which results in lower selectivity for epoxidation for both propylene and ethylene oxidation in the small size regime. The approach to steady state is fast in propylene oxidation (3–4 h) and is accompanied by changes in the UV–vis spectra that indicate a reduction in the Ag_2O phase. The approach to steady state is slow in ethylene oxidation (24–36 h) and is associated with changes in the UV–vis spectra that are consistent with the formation of a partially oxidized surface phase, which may involve subsurface or adsorbed oxygen.

Keywords: Propylene; Ethylene; Epoxidation; Silver; UV–vis spectroscopy

1. Introduction

Propylene oxide (PO) is an important commodity chemical used in the production of polyurethane, polyester resins, and surfactants, the production of which exceeded 5 million tons in 1999 [1]. The present major methods for PO production are the chlorohydrin process and variations of the Halcon process using *t*-butyl and ethylbenzene hydroperoxides. The chlorohydrin process produces large amounts of by-product salts and chlorinated organic compounds, and the hydroperoxide processes similarly produce a large quantity of coproducts (such as *t*-butylalcohol and styrene) [1]. Both processes suffer from plant complexity and marketing/production inefficiencies.

Several alternatives are being pursued to overcome the drawbacks in the present processes. A route recently commercialized by Sumitomo Chemical utilizes cumene hydroperoxide and recycles the alcohol formed in the epoxidation step so that there are no coproducts [2]. Other processes being developed by Lyondell and Bayer [3], BASF, Solvay and Dow [4], and Degussa and Krupp Uhde [5] use hy-

* Corresponding author.
E-mail address: oyama@vt.edu (S.T. Oyama).

0021-9517/$ – see front matter
doi:10.1016/j.jcat.2005.02.013

drogen peroxide (H_2O_2) produced captively in a separate plant. The H_2O_2 route was first demonstrated by Enichem with the use of a novel Ti-containing siliceous zeolite, TS-1 [6], and is attractive because it does not yield any coproducts. Currently, the catalyst for this route is titanium silicate with the TS-1 structure [7]. However, the H_2O_2 route is expensive, and improvements in the process are being studied, including in situ generation of H_2O_2 from H_2 and O_2 mixtures. Catalysts that have been investigated for simultaneous H_2O_2 formation and propylene epoxidation include palladium- or palladium/platinum-supported titanium silicalite [8–12], gold supported on titania [13], and gold supported on titanium silicates [14].

The discovery of a vapor-phase direct epoxidation catalyst capable of producing propylene oxide in higher selectivity than is currently attainable is most desirable. Silver is a well-known catalyst for ethylene epoxidation. However, the catalysts and reaction conditions that are best suited for ethylene oxide production do not give comparable selectivities in the direct epoxidation of propylene. There are various reports on the modification of silver catalysts to enhance the PO selectivity, in both the open [15–20] and patent [21–26] literature. Most of the silver catalysts for propylene epoxidation result in high silver loading, as well as heavy promotion. For example, a silver catalyst reported by ARCO contains 54 wt% silver mixed with $CaCO_3$ and is promoted with 0.5 wt% Mo and 2 wt% K. For a feed mixture containing 10% propylene, 5% oxygen, 200 ppm ethyl chloride, 75 ppm nitric oxide, 10% carbon dioxide, and the balance in nitrogen, at a gas hourly space velocity (GHSV) of 1200 h^{-1}, a total pressure of 0.21 MPa (30 psig), and 518 K (245 °C), the propylene conversion was 3.2% and the selectivity for PO was 58–59% [21]. It should be noted that a direct PO process would probably aim at high selectivity (80–90%) with low conversion (< 10%), as is practiced in EO production, so the results from ARCO are promising. Lambert et al. [19] studied the effect of Ag crystallite size in potassium-promoted $Ag/CaCO_3$ catalysts and found that the best PO selectivity of 15% was obtained on a catalyst containing a large proportion of Ag particles with sizes in the intermediate range of 20–40 nm. Ag particles that were either much smaller or much larger than this intermediate range were less selective toward epoxidation. However, almost all of the information regarding the structure and performance of ARCO-type catalysts (high silver content loaded on $CaCO_3$ with promoters) is found in patents, and few detailed studies have been made to help elucidate the nature of the active and selective sites for PO formation.

In situ diffuse reflectance spectroscopy in the ultraviolet–visible (UV–vis) region is useful for studying the electronic properties of heterogeneous catalysts and the nature of adsorbed intermediate species or side products during catalytic reactions [27–31]. More specifically, the optical properties of silver atoms, ions, and clusters have been well studied and exhibit characteristic UV–vis absorption bands [32]. Pestryakov et al. [33] have presented an interpretation of the UV–vis absorption bands of supported silver catalysts. Some of the most important spectral features include band transitions of Ag^+ at 6.5–5.4 eV (190–230 nm), Ag^0 at 5.0–3.8 eV (250–330 nm), and small Ag_n clusters at 3.8–3.4 and 2.8–2.3 eV (330–360 and 440–540 nm, respectively), and light absorption by large clusters (> 10 nm), crystallites, and aggregates mainly characterized by pronounced resonance lines due to collective excitations of conduction electrons at 3.1–2.4 eV (400–500 nm). These excitations are known as plasmon resonances, and their properties (i.e., spectral position, shape) can provide valuable information about the size, form, surrounding medium, and chemical interactions with the environment of the metal nanoparticles [32,34–41].

In this study we investigate the role of silver particle size in $Ag/CaCO_3$ catalysts for ethylene and propylene epoxidation and use scanning electron microscopy (SEM) and in situ UV–vis spectroscopy to examine the structure of the catalyst and the oxidation state of the catalyst surface.

2. Experimental

2.1. Catalyst preparation

A typical $Ag/CaCO_3$ catalyst was prepared as follows by a method similar to that reported by ARCO [21]. For a 56 wt% metal loading sample, 15 g (250 mmol) of ethylene diamine (Wako, 99.0%) and 10.1 g (112 mmol) of oxalic acid (Wako, 98.0%) were dissolved in 20 g of distilled, deionized H_2O, and 8.9 g (38.4 mmol) of Ag_2O (Wako, 99.0%) was slowly added to the mixture with magnetic stirring until it was completely dissolved. After 1 h of stirring, 1.8 g (29.5 mmol) of ethanol amine (Wako, 99.0%) was added to the mixture and stirred for another 1 h. Then 6.4 g (64 mmol) of $CaCO_3$ (Wako, 99.5%, specific area 0.5 $m^2\,g^{-1}$) was added to the solution to form a slurry. The slurry was transferred into a stainless-steel milling machine (Fritsch, model pulverisette 6) with 30 milling balls and was milled for 4 h. The milled sample was then dried at 393 K (120 °C) for 2 h and calcined at 633 K (360 °C) for 3 h. Samples with 0.5, 1, 7, 14, 28, and 42 wt% were prepared in a similar manner. In the designation $Ag(56)/CaCO_3$, the number in parentheses indicates the Ag loading in weight percent.

2.2. Catalytic testing

The epoxidation of propylene was carried out in a quartz tubular microreactor with a diameter of 6 mm and a length of 180 mm, with 0.5 g catalyst of 20–40 mesh size diluted with quartz sand of the same mesh size to a volume of 1 cm^3. Flow rates of He (Jorban Helium Supply, purity > 99.9%), O_2 (Hitachi Sanso, purity > 99.5%), and C_3H_6 (Takachiho Chemical, purity > 99.8%) were 15, 10, and 5 $cm^3\,min^{-1}$ each and were controlled by mass flow meters; the reaction pressure was set at 0.3 MPa. Before reaction the catalysts

were pretreated with He (15 $cm^3\,min^{-1}$) at 423 K (150 °C) for 1 h. Reaction products were analyzed online by two gas chromatographs (Shimadzu GC-14). One was equipped with a flame ionization detector (FID) and a thermal conductivity detector (TCD), which respectively included the use of a FFAP capillary column (0.32 mm × 60 m) and a Porapak Q compact column (3 mm × 2 m). The other had two TCDs attached to a MS-5A 60/80 compact column (3 mm × 2 m) and a Gaskuropak 54 84/100 compact column (3 mm × 2 m). The FFAP capillary column and Porapak Q column were used to detect oxygenates (acetaldehyde, PO, acetone, propionaldehyde, acrolein, acetic acid, and isopropanol) and CO_2, respectively, and the MS-5A and Gaskuropak columns were used to detect CO and hydrocarbons (propane, propylene, ethylene, and ethane), respectively. The compositions of the columns were as follows: FFAP, modified polyethylene glycol terephthalic acid; Poropak Q, ethylvinylbenzene–divinylbenzene porous polymers; MS-5A, molecular sieve 5A, Gaskuropak 54 80/100, polystyrene-divinylbenzene porous polymer 80–100 mesh. Carbon balances closed to 100 ± 3%. The epoxidation of ethylene was carried out in an identical manner, except that ethylene (Takachiho Chemical, purity 99.5%) was used as a reactant.

2.3. X-Ray diffraction, O_2 chemisorption, FESEM, and in situ UV–vis measurements

The X-ray diffraction patterns of the samples were obtained with an X-ray diffractometer (Rigaku, RINT2000) operated at 40 kV and 40 mA, with Cu-K_α monochromatized radiation ($\lambda = 0.154178$ nm). Crystallite sizes (D_c) of the catalysts were determined from the line broadening of the two most intense peaks at $2\theta = 64.4°$ and $2\theta = 77.4°$, with the use of the Scherrer equation, $D_c = K\lambda/\beta\cos(\theta)$, where K is a constant taken as 0.9, λ is the wavelength of the X-ray radiation, β is the width of the peak at half-maximum corrected for instrumental broadening (0.1°), and 2θ is the Bragg angle [42].

Surface areas and oxygen uptakes were measured in a volumetric adsorption unit (Micromeritics ASAP 2020). For the chemisorption measurements the samples were heated in flowing O_2 for 1 h, evacuated for 0.5 h, reduced in flowing H_2 for 1 h, evacuated to < 1.3 mPa (10 μm Hg) for 0.5 h, and dosed with O_2, all at 443 K (170 °C). Silver particle size and metallic surface area were calculated from the O_2 chemisorption uptake (μmol g^{-1}). Based on an adsorption stoichiometry of $O_{ad}/Ag_s = 1$, where Ag_s represents a surface Ag atom, dispersion for the silver samples can be calculated by dividing the number of chemisorbed O atoms by the total number of Ag atoms [43–45], and if spherical Ag crystallites are assumed, the relationship between crystallite size and dispersion, D, is d (nm) = 1.34/D [43,46,47]. The metallic surface area was calculated according to the equation S ($m^2\,g^{-1}$) = (O_2 uptake × 2 × 10^{-6} × 6.02 × 10^{23})/1.14 × 10^{19}, where 6.02 × 10^{23} is Avogadro's constant and 1.14 × 10^{19} m^{-2} is the surface density of silver atoms averaged for the three low index planes (100), (110), and (111).

Field emission scanning electron microscopy (FESEM) images of the samples were obtained in a microscope (JEOL JSM 6500) operated at 15 kV. We obtained particle size distributions by measuring the diameters of at least 20 particles in a representative region.

In situ UV–vis spectra were collected with a large-compartment spectrometer (Varian Cary 5000) equipped with a reaction chamber (Harrick Scientific; model HVC-DRP) in conjunction with a praying mantis diffuse reflectance attachment (DRP-XXX). Initially, the catalysts were pretreated as for the reaction studies with He (15 $cm^3\,min^{-1}$) at 423 K (150 °C) for 1 h and were then cooled to 298 K (25 °C). The flow was then switched to reaction gases at the same flow rate (C_3H_6 or C_2H_4 = 5 $cm^3\,min^{-1}$, O_2 = 10 $cm^3\,min^{-1}$, He = 15 $cm^3\,min^{-1}$) and pressure (0.3 MPa) as in the reaction studies. Then the reaction temperature was raised to 473 K (200 °C) at a rate of 0.17 $K\,s^{-1}$ (10 $K\,min^{-1}$), and spectra were recorded after 1 h over the range of 200–800 nm at a scan rate of 200 nm min^{-1}, an average time of 0.5 s, and a data interval of 0.333 nm. Spectra were referenced to $CaCO_3$ under the same reaction conditions (pretreatment, gas environment, pressure, and temperature). Diffuse reflectance spectra were analyzed with the use of the Kubelka–Munk function, $F(R_\alpha)$, calculated from the absorbance data [48].

3. Results

3.1. XRD, SEM, and O_2 chemisorption measurements

Fig. 1 shows the XRD patterns of the Ag/$CaCO_3$ catalysts with different silver loading. The main peaks at 23.1, 29.5, 31.8, 36.1, 39.6, 43.3, 47.6, 48.5, 57.5, and 60.9° (2θ) are due to the $CaCO_3$ support. With increasing silver loading, the intensities of peaks due to crystalline silver at 38.3, 44.3, 64.7, and 77.6° (2θ) grow from very faint and diffuse for the 0.5 wt% sample to very strong and sharp for the 56 wt% sample.

Fig. 2 presents the FESEM images of silver catalysts with 1, 14, and 56 wt% silver. The silver particle increases in size and the distribution becomes broader with silver loading level. For the 1, 14, and 56 wt% samples the maxima in the distributions are 50, 170, and 370 nm, respectively, and the breadths are approximately 20, 50, and 300 nm. With increasing loading there is evidence for particle agglomeration and irregular particle shape.

Table 1 summarizes O_2 chemisorption and surface area results for the Ag catalysts. The O_2 uptakes initially increased rapidly with the Ag loading levels but then leveled off, reaching a maximum of 5.9 μmol g^{-1} for a loading of 42 wt%, and then decreased. The Ag particle size calculated from the chemisorption values increased with Ag loading,

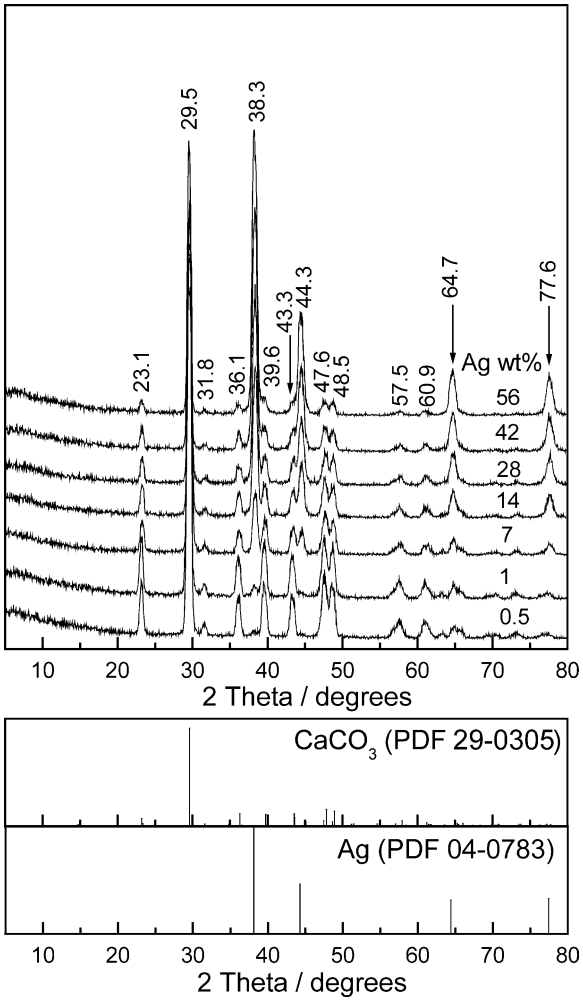

Fig. 1. XRD patterns of Ag(x)/$CaCO_3$ catalysts and references.

from 50 to 660 nm for silver loadings of 0.5 to 56 wt%. The total specific surface area decreased slightly with loading.

3.2. Catalytic testing

Fig. 3 shows the propylene epoxidation results over 0.5-g samples of the Ag(x)/$CaCO_3$ catalysts. No products other than PO, CO_2, and H_2O were found. Propylene conversion increased with temperature and silver loading; a lower temperature was required to obtain the same conversion at higher silver content. PO selectivity decreased with increasing temperature; the decline was very pronounced at conversions greater than 30% for all of catalysts. The highest PO selectivity was only about 10% and was obtained when the conversion was low.

Fig. 4 shows the ethylene epoxidation results over 0.5-g samples of the Ag/$CaCO_3$ catalysts. The trends in the ethylene conversion were the same as for propylene, with conversion increasing with silver loading. However, the conversions for the high loading catalysts were close to each other and higher than in the case for propylene. The EO selectivity was much higher than the PO selectivity for each catalyst, with the highest EO selectivity attaining 70%. The selectivity results fell into two regions. For loadings higher than 7 wt%, the selectivities were close to each other but generally fell with increasing loading. Small discrepancies in order are due to experimental error. For the low loading of 0.5 and 1 wt%, the selectivities were substantially higher and increased for the higher loadings.

Fig. 5a shows a typical time course for propylene epoxidation over a Ag/$CaCO_3$ catalyst (14 wt%). After a short induction period of 3–4 h, the catalyst shows stable reactivity for more than 25 h with a propylene conversion of 15% and a PO selectivity of about 8%. However, the performance is quite different for ethylene epoxidation. Fig. 5b shows that ethylene conversion gradually declined with reaction time, before becoming steady, starting at around 24–36 h, whereas the EO selectivity went up. The catalyst stabilized with an ethylene conversion of 9% and an EO selectivity of 53%.

3.3. In situ UV–vis spectroscopy

Figs. 6 and 7 present in situ UV–vis spectra for Ag/$CaCO_3$ catalysts with different silver loadings for propylene and ethylene epoxidation at 473 K (200 °C), respectively. From a comparison of the two figures, it can be seen that there are no appreciable differences between the spectra for the same silver loading after 1 h on stream. Three main features could be identified: silver plasmon resonances (2.4–3.7 eV), Ag^0 band transitions (3.8–4.6 eV), and Ag^+ band transitions

Table 1
Comparison of surface properties of Ag(x)/$CaCO_3$ catalysts

Ag loading (wt%)	O_2 uptake (μmol g^{-1})	Metallic surface area (m^2 g^{-1})	D_{chem}[a] (nm)	D_{SEM}[b] (nm)	XRD crystallite size[c] (nm)	BET surface area (m^2 g^{-1})
0.5	0.663	0.070	49	–	7.85	–
1	0.943	0.099	66	50	10.0	6.5
7	2.916	0.307	149	–	13.2	–
14	4.522	0.476	192	170	13.6	3.3
28	4.633	0.488	375	–	13.6	–
42	5.941	0.626	439	–	13.6	–
56	5.297	0.558	656	370	14.2	3.0

[a] Calculated from oxygen chemisorption uptakes.
[b] Calculated from scanning electron microscopy.
[c] Calculated by the Scherrer equation.

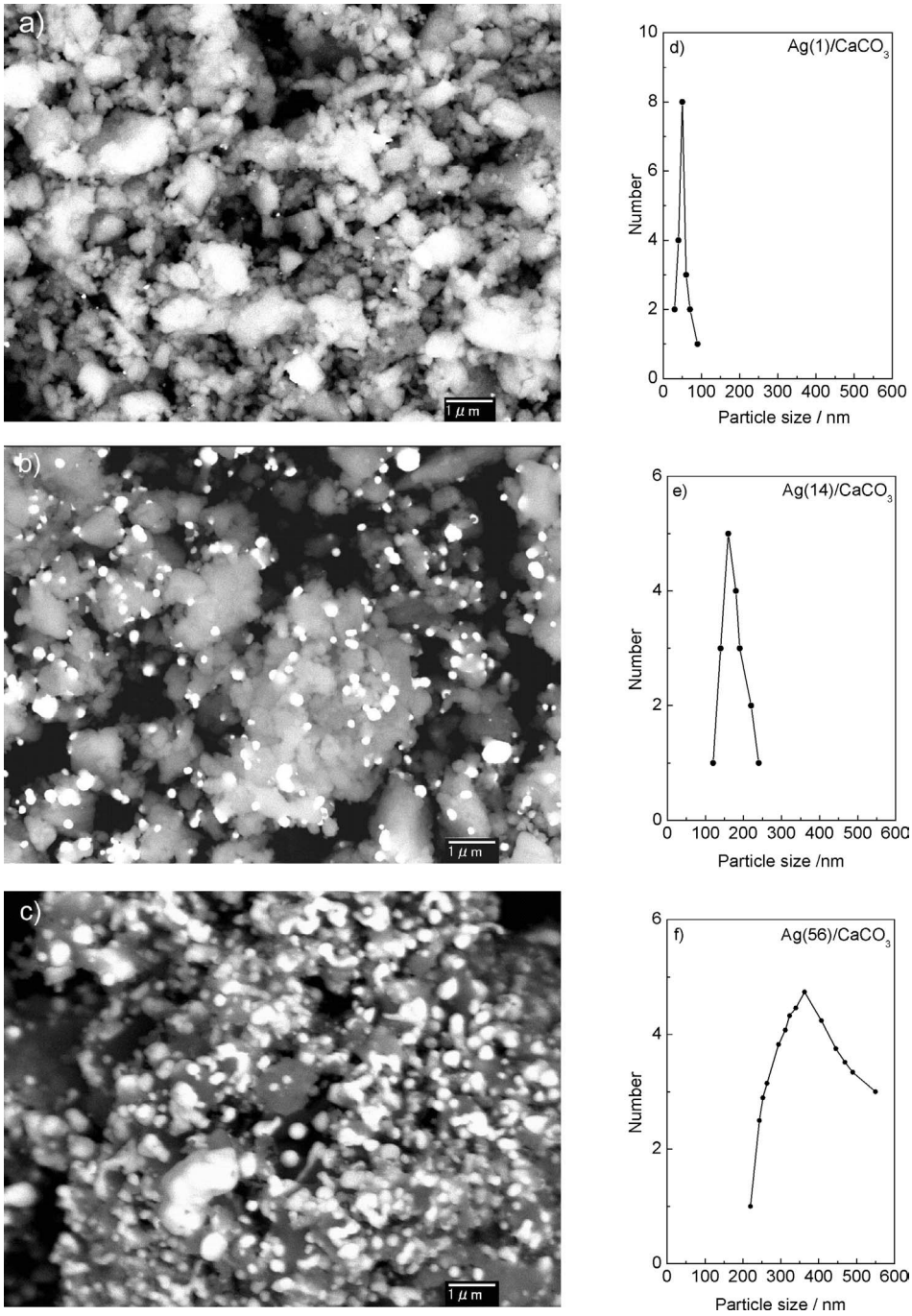

Fig. 2. Field emission scanning electron microscopy (FESEM) images (left) and particle size distribution (right) of Ag(x)/$CaCO_3$ catalysts. Left: (a) Ag(1)/$CaCO_3$, (b) Ag(14)/$CaCO_3$, (c) Ag(56)/$CaCO_3$. Right: (d) Ag(1)/$CaCO_3$, (e) Ag(14)/$CaCO_3$, (f) Ag(56)/$CaCO_3$.

(5.4–6.2 eV). Figs. 6 and 7 show that the plasmon resonance was quite symmetric and was centered at around 3.0 eV for the catalysts up to 7 wt% silver loading. For silver loadings higher than 14 wt%, the plasmon resonance was no longer symmetric, and two changes could be noticed: a shift of the main plasmon resonance peak to higher energies (blue shift) at around 3.2 eV, and the appearance of a shoulder at about 3.5 eV. The intensity of Ag^0 band transitions increased proportionally with the silver loading in the catalysts, as expected. In the case of Ag^+ band transitions, the intensity dependence on silver loading could not be ascertained exactly because of the change in background; however, there is a clear trend of increasing Ag^+/Ag^0 ratio with decreasing silver loading.

Figs. 8 and 9 present in situ UV–vis spectra for Ag(14)/$CaCO_3$ catalyst with time on stream at 493 K (200 °C) and 0.3 MPa in C_3H_6/O_2/He and C_2H_4/O_2/He, respectively. In the case of propylene epoxidation (Fig. 8), the most remarkable change was the quick reduction of the feature due to Ag^+ band transitions, which occurred rapidly up to 4.5 h on

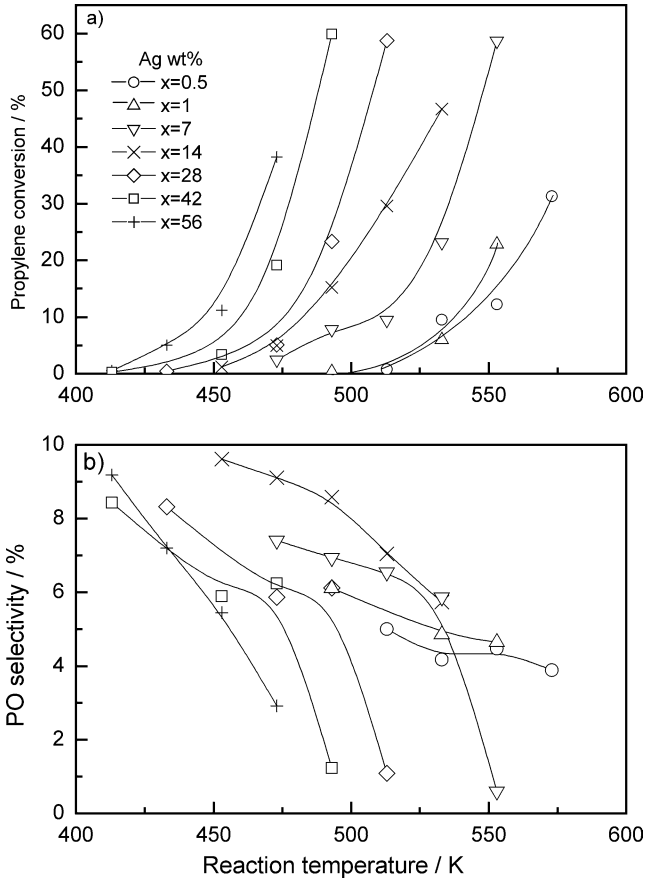

Fig. 3. Propylene epoxidation over Ag(x)/$CaCO_3$ catalysts (a) propylene conversion, (b) PO selectivity.

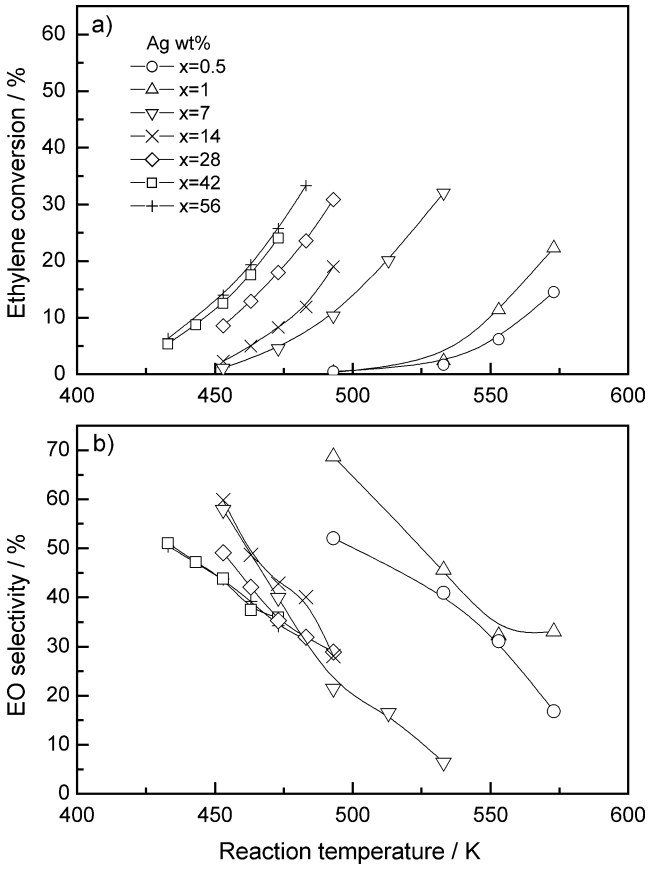

Fig. 4. Ethylene epoxidation over Ag(x)/$CaCO_3$ catalysts (a) ethylene conversion, (b) EO selectivity.

stream and was fairly complete after 8.5 h (see dashed arrow for extrapolated baseline). After 24 h, only a slight shift to lower energy (red shift) of the main plasmon resonance position and other minor changes were observed (solid arrow). In the case of ethylene epoxidation (Fig. 9) there was again a decrease in the intensity of the Ag^+ feature, but in this case the reduction process was slower than that in the propylene epoxidation. Even after 24–36 h on stream, the Ag^+ feature was still present (considerable intensity remained above the dashed arrow). On the other hand, the main plasmon resonance position was significantly shifted to lower energies (red shift) together with other changes (solid arrow).

4. Discussion

In this work a series of Ag/$CaCO_3$ catalysts with silver loadings from 0.5 to 56 wt% were used to study the effect of particle size on the epoxidation reactions of ethylene and propylene with molecular oxygen. The total surface area of the catalysts was low, 3–6 $m^2\,g^{-1}$ (Table 1), as is typical for this type of material. In the catalysts the silver particle size becomes larger with increasing loading, as indicated by XRD, SEM, and O_2 chemisorption data. The XRD patterns (Fig. 1) show that the peak intensities due to crystalline silver become stronger and sharper as the silver content is increased, indicating that the silver particles grow with an increase in loading. This trend is supported by the SEM observations (Fig. 2). The Ag(1)/$CaCO_3$ sample displays small silver particles on the support, which grow in size for the Ag(14)/$CaCO_3$ sample and become larger and more numerous for the Ag(56)/$CaCO_3$ sample. The particle size distribution is narrow for the low loading sample and increases in breadth for the high loading samples. Furthermore, the micrographs show that the low loading samples present silver particles that are close to spherical in shape, whereas the high loading samples have silver particles of irregular morphology as the particles agglomerate and coalesce. These results will be quantified shortly.

The particle shape trends are also indicated by the UV–vis results. The fact that the plasmon resonance is quite symmetric and is centered at around 3.0 eV for the samples up to 7 wt% silver loading indicates that the silver particles have a regular spherical shape of narrow size distribution. For samples with higher silver loading, the presence of a new peak in the plasmon feature (resonance of higher multipolar order) indicates the presence of oblate spheroids and large clusters in which the optical field becomes non-uniform across the cluster [32,36,40,49]. These resonances at about 3.2 and 3.5 eV are referred to as the (1, 1) and (1, 0) modes, re-

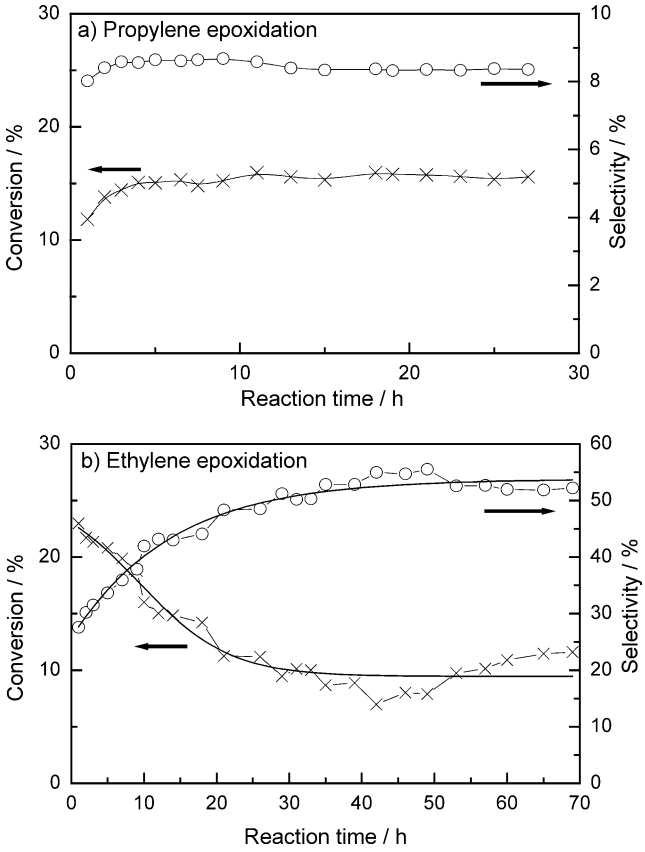

Fig. 5. Time course of propylene and ethylene epoxidation over the $Ag(14)/CaCO_3$ catalyst: (a) propylene epoxidation, (b) ethylene epoxidation. Reaction temperature, 493 K (220 °C).

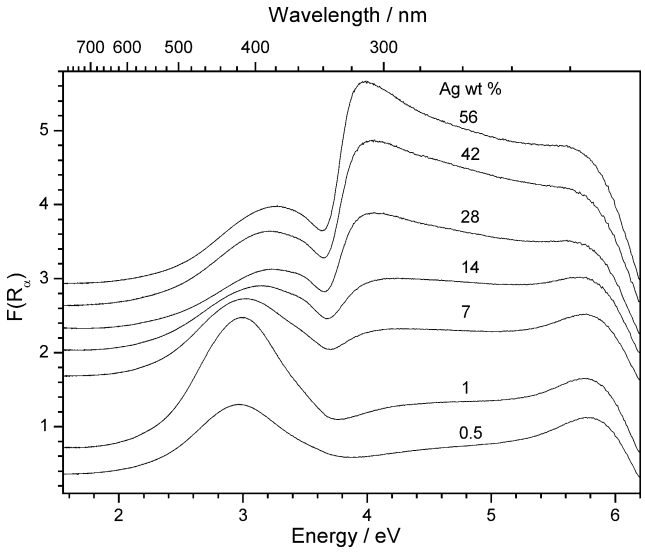

Fig. 6. In situ UV–vis diffuse reflectance spectra of $Ag/CaCO_3$ catalysts with different silver loadings at 473 K (200 °C) and 0.3 MPa in C_3H_6/O_2/He. Offsets are used for clarity.

spectively. The (1, 1) mode is due to excitation of plasmon polaritrons in the direction of the particle long axis (b), and the (1, 0) mode is due to the excitation of collective oscillations in the direction of the particle short axis (a). The

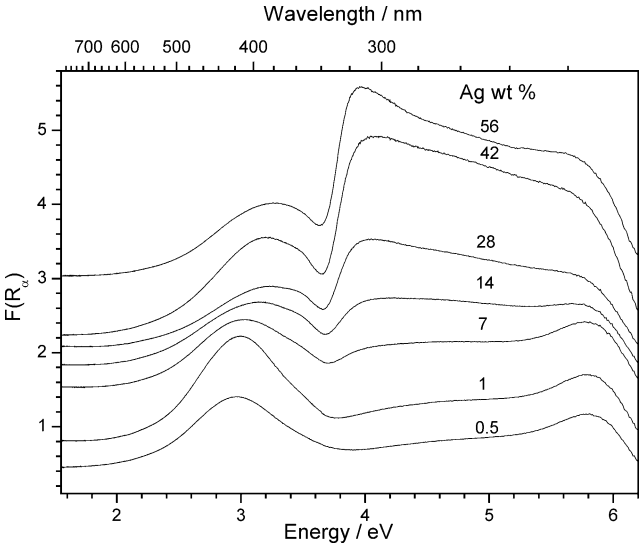

Fig. 7. In situ UV–vis diffuse reflectance spectra of $Ag/CaCO_3$ catalysts with different silver loadings at 473 K (200 °C) and 0.3 MPa in C_2H_4/O_2/He. Offsets are used for clarity.

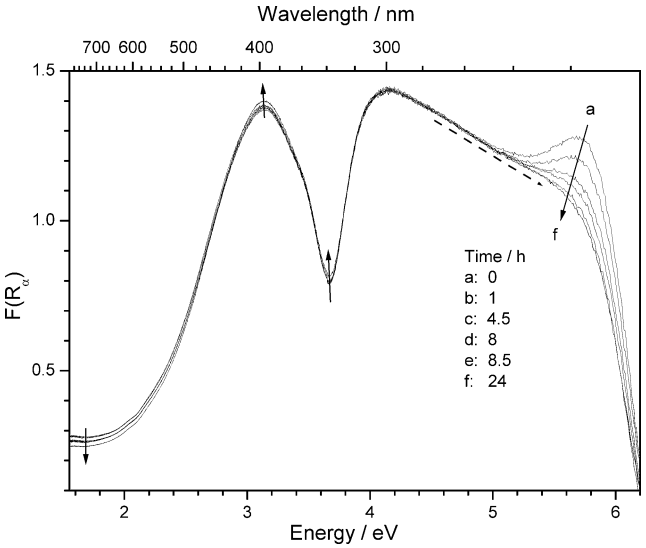

Fig. 8. In situ UV–vis diffuse reflectance spectra of $Ag(14)/CaCO_3$ catalyst with time on stream at 493 K (220 °C) and 0.3 MPa in C_3H_6/O_2/He.

positions of these resonances depend on the ratio a/b (for completely spherical particles the ratio a/b is 1) and are a function of the particle shape. For instance, the larger the ratio of the peak positions (in eV) of the (1, 0)/(1, 1) modes, the smaller the ratio a/b [36,49]. Therefore, it can be said that for $Ag(x)/CaCO_3$ catalysts with silver loading higher than 14 wt%, the silver particles have larger sizes and are no longer spherical, tending to form oblate spheroids.

The results of O_2 chemisorption on $Ag/CaCO_3$ catalysts show that for catalysts with silver loading higher than 14 wt%, O_2 uptake increased, but not proportionally to the loading. This also indicates that there is crystallite agglomeration on the high loading samples, resulting in a poorer dispersion of Ag particles, hence giving lower O_2 chemisorp-

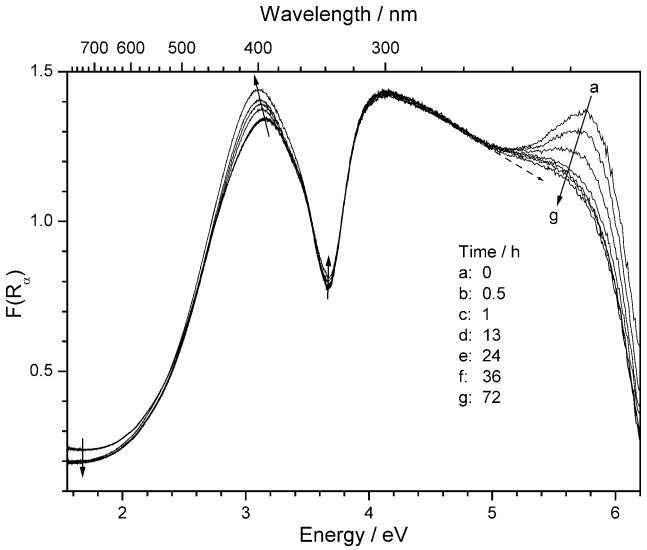

Fig. 9. In situ UV–vis diffuse reflectance spectra of $Ag(14)/CaCO_3$ catalyst with time on stream at 493 K (220 °C) and 0.3 MPa in $C_2H_4/O_2/He$.

tion. Such sintering of silver particles is well known. Ruckenstein and Lee [50] reported crystallite migration and coalescence when Ag samples were heated in O_2 for silver particles supported on nonporous alumina, which was found by transmission electron microscopy. The $Ag(14)/CaCO_3$ sample shows 4.5 μmol g^{-1} O_2 uptake, which is consistent with previous results of Badani and Vannice [51]. Badani and Vannice prepared an Ag/α-Al_2O_3 catalyst with 15.1 wt% silver loading, which had an O_2 uptake of 4.4 μmol g^{-1}. The particle size in the $Ag(14)/CaCO_3$ sample is in the same range as that of their $Ag(15)/\alpha$-Al_2O_3 sample, which gives an average particle size of 213 nm, calculated by O_2 chemisorption uptake. Results for other loadings are summarized in Table 1. There is good agreement between the particle size measured by O_2 chemisorption and those determined from the SEM pictures. For the 1, 14, and 56 wt% samples the O_2 chemisorption values are 66, 192, and 656 nm, whereas the SEM values are 50, 170, 370 nm. Note that the particle sizes calculated with the Scherrer equation are much smaller than those obtained by SEM and by O_2 chemisorption. This may be due to the low sensitivity of the line-broadening technique to large crystallites and to strains in the large Ag particles [52], but most likely is due to the presence of polycrystalline aggregates.

It should be noted that although O_2 chemisorption is used in this study to estimate the number of surface sites, as with all chemisorption techniques the results are approximate. This is particularly the case for silver in which subsurface oxygen chemisorption and bulk oxidation may occur at higher oxygen coverages [53]. However, the good agreement between the chemisorption and SEM techniques gives credence to the assumption that in this case the approximation is reasonable.

UV–vis spectroscopy can also provide information about the surface oxidation state of the silver particles. As discussed earlier, the features at intermediate energy (3.8–4.6 eV) are due to band transitions of metallic Ag^0, and the features at high energy (5.4–6.2 eV) are due to electronic transition involving the Ag^+ ion. It is clear from the results in Figs. 6 and 7 that the ratio Ag^+/Ag^0 increased with lower silver loading. The results indicate that all particles have some oxide present and that the smaller silver particles have a larger proportion of the oxide. This is in accordance with a thermodynamic analysis at atmospheric pressure of the free energy of formation of Ag_2O (in kJ mol^{-1}) from spherical silver particles, which resulted in the equation $Ag + O_2 \rightarrow Ag_2O$, $\Delta G^0_{298\ K} = -11.25 - 115.0/D$, where D is the particle diameter in nanometers [54]. The equation predicts that smaller silver particles are more easily oxidized. It is likely that the oxide is in the form of a thin layer on the surface of a metallic core, as the XRD results show strong metal peaks but no oxide features.

Table 2
PO and EO selectivities for $Ag/CaCO_3$ catalysts at propylene and ethylene conversions of 10%

Catalyst	PO formation		EO formation	
	Temperature (K)	Selectivity (%)	Temperature (K)	Selectivity (%)
$Ag(56)/CaCO_3$	445	6.0	441	48.0
$Ag(42)/CaCO_3$	460	6.1	445	46.1
$Ag(28)/CaCO_3$	474	6.2	456	46.7
$Ag(14)/CaCO_3$	483	8.9	477	41.6
$Ag(7)/CaCO_3$	508	6.7	489	25.7
$Ag(1)/CaCO_3$	535	5.0	550	32.0
$Ag(0.5)/CaCO_3$	540	4.3	562	24.7

The different catalytic behaviors of the $Ag/CaCO_3$ catalysts for propylene (Fig. 3) and ethylene (Fig. 4) epoxidation are understandable. The low PO selectivity on the silver catalysts is known to be due to the reaction between allylic hydrogens and adsorbed nucleophilic oxygen species, which results in total combustion [55–57]. Table 2 lists PO and EO selectivities for $Ag/CaCO_3$ catalysts at propylene and ethylene conversions of 10% each. It can be seen that for propylene and ethylene the conversion behavior is similar. Higher reaction temperatures are needed for catalysts with low silver loading to obtain the same conversion. The selectivity results show some differences, however. The selectivity for PO is low and relatively constant, increasing slightly for catalysts with intermediate loading centered at $Ag(14)/CaCO_3$. The selectivity for EO is highest for the catalyst with the highest loading and decreases with loading. The decline in EO selectivity is more pronounced than that in PO. These results suggest that for both propylene and ethylene epoxidation, large silver particles are favorable, and ethylene epoxidation is more sensitive to the silver particle than propylene epoxidation is. This conclusion for EO is well known, as the best catalysts are recognized to have low surface area and massive silver crystallites [58,59].

To compare the intrinsic activities of the $Ag/CaCO_3$ samples with different Ag loading, turnover frequencies (TOFs)

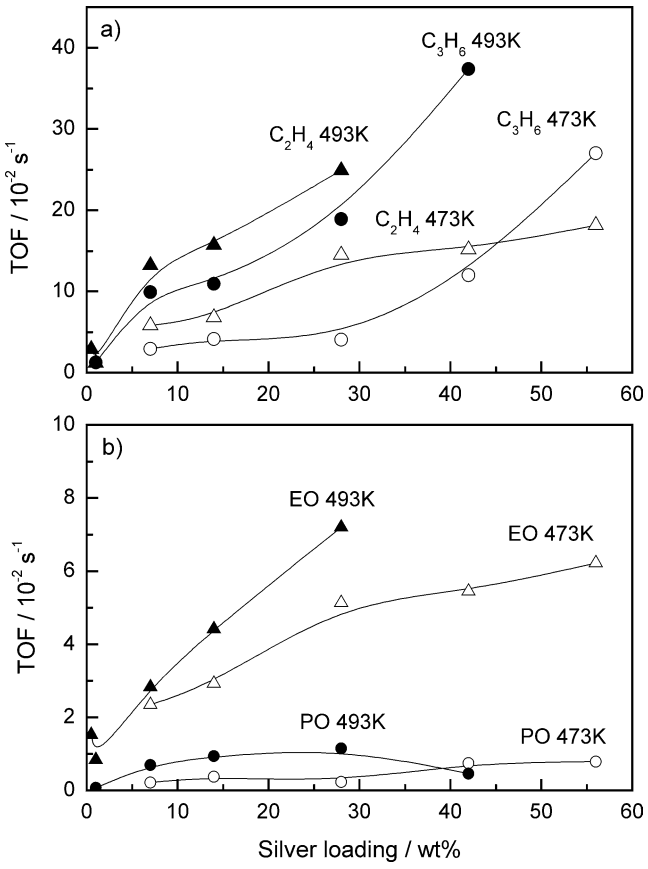

Fig. 10. Turnover frequencies (TOF) for total reaction (a) and PO and EO formation (b).

for total reaction and EO and PO formation were calculated at 473 and 493 K based on the oxygen chemisorption uptakes (Fig. 10). Reaction rates for both ethylene and propylene increase with reaction temperature. For PO formation the TOF increased slightly with silver loading at both temperatures. For EO formation, the TOF increased fivefold for catalysts with 1 to 28 wt% silver loading at 493 K (220 °C) (particle size ranging from 70 to 380 nm) and threefold at 473 K (200 °C). Classically, particle size effects can be used to determine the structure-sensitivity of reactions [60]. The present finding that the PO formation rate does not change with Ag particle size whereas the EO formation rate varies indicates that propylene epoxidation is structure-insensitive, whereas ethylene epoxidation is structure-sensitive, at least with Ag particle sizes ranging from 50 to 660 nm. However, these conclusions, especially for the case of PO, need to be qualified because of various complicating factors. First, the epoxidation of propylene occurs with very low selectivity, and it is doubtful that a firm conclusion about the effect of structure can be reached when the reaction pathway being examined is minor compared with others. Second, the changes in the structure of the catalysts are not as large as should be expected because their size range is limited, especially on the low side. Normally, large changes are expected in the range of 1–10 nm [61], which is not attained in the present study. In addition, the occurrence of particle agglomeration at the larger loadings probably increases surface disorder in those samples and offsets the expected gains in the proportion of smooth surfaces. This helps explain the limited changes in TOF in both reactions. Still another factor, and perhaps the most important, is the change in oxidation state of the silver particles with size. The UV–vis measurements at reaction conditions clearly indicate that the smaller particles have larger amounts of Ag^+ species than the larger particles. The smaller particles are probably partially covered with a layer of Ag_2O. In the case of ethylene this compound has been reported to yield less EO [62]. Thus, the observed decline in EO TOF (Fig. 10) with a decrease in particle size is likely to be due to a change in the active phase from metallic to oxidic rather than a purely structural change in going to small particles. The lack of change in PO selectivity may be due to the fact that the total oxidation reaction occurs readily in both the metallic and oxidic phases.

Another interesting finding in this study is the transient behavior of propylene and ethylene epoxidation on the $Ag(14)/CaCO_3$ catalyst. It was found that propylene epoxidation reached steady state within 4–5 h, whereas ethylene epoxidation required about 24–36 h to reach a constant state. This is probably related to changes in the catalyst surface during reaction. For the propylene reaction the in situ UV–vis spectra showed a relatively fast reduction of the high-energy (5.2–6.4 eV) Ag^+ peak, with the peak reaching a constant value after 4–5 h. In contrast, for the ethylene reaction the Ag^+ peak was reduced and reached a steady value after 24–36 h. Clearly, there is a very good correspondence between the reactivity results and the UV–vis data. The decrease in the intensity of the Ag^+ peaks during propylene and ethylene epoxidation has a direct relationship with the reactivity. Upon exposure to the reactive gas mixture in both propylene and ethylene oxidation, the silver particles interact strongly with oxygen and, for the thermodynamic reasons discussed earlier, form a surface Ag_2O layer. As the reaction proceeds, the propylene and ethylene react with the surface oxygen species and gradually reduce the surface. The total rates of reaction in the two cases are similar (Fig. 10a). For the $Ag(14)/CaCO_3$ sample at 493 K the total turnover frequencies are, respectively, 0.10 s^{-1} (for propylene oxidation) and 0.15 s^{-1} (for ethylene oxidation), with corresponding characteristic times ($t = 1/\text{TOF}$) of 10 s and 6.7 s. Thus, changes in the catalyst surface occur over many turnovers. In the case of propylene the changes occur rapidly, probably because the selectivity for deep oxidation is much higher and much more surface oxygen is consumed in each catalytic cycle. It is evident that propylene has a stronger reducing ability than ethylene and is able to reduce the surface Ag_2O faster during reaction. The Ag_2O is almost completely reduced during propylene epoxidation (Fig. 8), whereas it is partially reduced during ethylene epoxidation (Fig. 9). The reducing capability of propylene has been investigated on silver catalysts in the selective oxidation of NO to NO_2. Bogdanchikova et al. [63] found that in selective catalytic reduc-

tion (SCR) a feed containing 500 ppm of propylene in a large excess of O_2 reduced part of the oxidized silver species. They suggested that the high affinity of the π-electrons of propylene for metal cations probably favored the adsorption of the hydrocarbon to the catalyst and allowed the reduction, despite the presence of O_2.

Another significant change revealed by the in situ UV–vis spectra is the occurrence of a red shift of the main silver plasmon resonance position during ethylene epoxidation (Fig. 9). This is not observed in propylene epoxidation. The change for the ethylene reaction may be related to a variation in the shape of the silver particles from spherical to oblate spheroids [37]. Ruckenstein and Lee [50] found that when silver particles were heated in C_2H_4 the particles changed their shape from circular to ellipsoidal, and when heated in a mixture of C_2H_4 and O_2 the particles acquired more irregular shapes. It is possible that during ethylene oxidation the particles undergo restructuring [64] that gives rise to the observed change in the silver plasmon resonance. This restructuring may be associated with the formation of a unique surface phase active for the EO reaction. There are two possibilities for this phase. One of them is a phase containing subsurface oxygen and the other is a phase with an optimal amount of adsorbed oxygen. Subsurface oxygen was first suggested by van Santen and Kuipers [65] to explain a variety of results in the EO literature and has been used to explain other features of the reaction, such as isotopic exchange, effect of promoters, transient use of oxygen inventories, and microkinetic analysis [66–68]. A slow process would seem to be more consistent with the formation of a subsurface oxygen phase. Adsorbed oxygen has been suggested to give selective epoxidation of ethylene by Kazanski et al. [69] and in more recent work detailing the existence of nucleophilic (nonselective) and electrophilic (selective) adsorbed atomic oxygen [70,71]. Although the UV–vis results cannot give unequivocal evidence for the existence of either phase, it does demonstrate that during ethylene oxidation the catalyst achieves a state of partial oxidation in a slow process, whereas during propylene oxidation it reaches a more reduced condition in a fast process.

5. Conclusion

This work has examined the effect of particle size on the reactivity behavior of $Ag/CaCO_3$ catalysts in the epoxidation of propylene and ethylene. It was found that propylene epoxidation at 473–493 K was relatively insensitive to particle size. However, this may have been due to the low intrinsic selectivity of the silver catalysts for propylene oxide ($< 10\%$), with structural effects being dominated by the complete combustion reaction. In contrast, it was found that ethylene epoxidation exhibited mild structure sensitivity, with the turnover frequency decreasing by three- to fivefold as the particle size decreased from 660 to 50 nm. Particle sizes in this study were calculated from oxygen chemisorption uptakes, assuming equal numbers of low index planes were exposed. Particles sizes obtained from field emission scanning electron microscopy gave good agreement with the calculated particle sizes and showed the occurrence of particle agglomeration at high loadings. UV–vis reflectance spectroscopy confirmed these results, indicating the presence of spherical particles at low loading and larger less symmetric shapes at high loadings. The UV–vis spectroscopy also supported the findings by X-ray diffraction that the silver was mostly metallic, but also showed the presence of an oxide phase with a Ag^+ component that was more favored with lower particle sizes. Transient results indicated that propylene oxidation reached steady state quickly (3–5 h), and parallel UV–vis spectra showed substantial reduction of the oxidic component. In the case of ethylene oxidation, steady state was attained slowly (24–36 h), and UV–vis spectra indicated retention of the oxidic component, with other spectral changes consistent with the possible presence of adsorbed or subsurface oxygen.

Acknowledgments

The authors are grateful for financial support from the Ministry of Economy, Trade and Industry (METI) (Minimum energy chemistry project) and the National Science Foundation under grant CTS-0321979.

References

[1] D.L. Trent, Propylene Oxide, in: Kirk Othmer Encyclopedia of Chemical Technology, online ed., Wiley, New York, 2001.
[2] T. Seo, J. Tsuji, US Patent 6,646,139 (November 11, 2003), to Sumitomo Chemical Company.
[3] A. Wood, Chem. Week 164 (41) (2002) 26.
[4] A. Tullo, Chem. Eng. News 6 (2004) 15.
[5] P. Raleigh, Urethanes Technology 20 (3) (2003) 3.
[6] M.G. Clerici, G. Bellussi, U. Romano, J. Catal. 129 (1991) 159.
[7] J.H. Teles, A. Rehfinger, P. Bassler, A. Wenzel, N. Rieber, P. Rudolf, US Patent 6,756,503 (June 29, 2004), to BASF Aktiengesellschaft.
[8] A. Sato, T. Miyake, Japan Patent 4,352,771 (December 7, 1992), to Tosoh.
[9] A. Sato, M. Oguri, M. Tokumaru, T. Miyake, Japan Patent Appl. 269,029 (October 15, 1996), to Tosoh.
[10] A. Sato, M. Oguri, M. Tokumaru, T. Miyake, Japan Patent Appl. 269,030 (October 15, 1996), to Tosoh.
[11] M. Fisher, P. Lingelbach, U. Muller, N. Rieber, P. Bassler, J. Dembowski, K. Eller, W. Harder, V. Kohl, German Patent Appl. DE 44 25 672 Al (January 25, 1996), to BASF AG.
[12] R. Meiers, U. Dingerdissen, W.F. Hölderich, J. Catal. 176 (1998) 376.
[13] T. Hayashi, K. Tanaka, M. Haruta, J. Catal. 178 (1998) 566.
[14] A.K. Sinha, S. Seelan, S. Tsubota, M. Haruta, Angew. Chem. Int. Ed. 43 (2004) 1546.
[15] G. Lu, X. Zuo, Catal. Lett. 58 (1999) 67.
[16] J. Lu, M. Luo, H. Lei, C. Li, Appl. Catal. A 237 (2002) 11.
[17] M. Luo, J. Lu, C. Li, Catal. Lett. 86 (2003) 43.
[18] A. Palermo, A. Husain, M. Tikhov, R. Lambert, J. Catal. 207 (2002) 331.
[19] F. Zemicheael, A. Palermo, M. Tikhov, R. Lambert, Catal. Lett. 80 (2002) 93.

[20] G. Jin, G. Lu, Y. Guo, J. Wang, X. Liu, Catal. Lett. 87 (2003) 249.
[21] R. Pitchai, A.P. Kahn, A.M. Gaffney, US Patent 5,625,084 (April 29, 1997), to ARCO Chemical Technology, L.P.
[22] R. Pitchai, A.P. Kahn, A.M. Gaffney, US Patent 5,686,380 (November 11, 1997), to ARCO Chemical Technology, L.P.
[23] A.M. Gaffney, C.A. Jones, R. Pitchai, A.P. Kahn, US Patent 5,698,719 (December 16, 1997), to ARCO Chemical Technology, L.P.
[24] A.M. Gaffney, A.P. Kahn, R. Pitchai, US Patent 5,703,254 (December 30, 1997), to ARCO Chemical Technology, L.P.
[25] B. Cooker, A.M. Gaffney, J.D. Jewson, A.P. Kahn, R. Pitchai, US Patent 5,770,746 (June 23, 1998), to ARCO Chemical Technology, L.P.
[26] B. Cooker, A.M. Gaffney, J.D. Jewson, W.H. Onimus, US Patent 5,780,657 (July 14, 1998), to ARCO Chemical Technology, L.P.
[27] B.M. Weckhuysen, R.A. Schoonheydt, Catal. Today 49 (1999) 441.
[28] J. Melsheimer, M. Thiede, R. Ahmad, G. Tzolova-Müller, F.C. Jentoft, Phys. Chem. Chem. Phys. 5 (2003) 4366.
[29] X. Gao, J.-M. Jehng, I.E. Wachs, J. Catal. 209 (2002) 43.
[30] M.D. Argyle, K. Chen, C. Resini, C. Krebs, A.T. Bell, E. Iglesia, J. Phys. Chem. B 109 (2004) 2345.
[31] R. Ahmad, J. Melsheimer, F.C. Jentoft, R. Schlögl, J. Catal. 218 (2003) 365.
[32] U. Kreibig, M. Vollmer, Optical Properties of Metal Clusters, Springer, Berlin, 1995.
[33] A.N. Pestryakov, A.A. Davydov, J. Electron. Spectrosc. Relat. Phenom. 74 (1995) 195.
[34] K.L. Kelly, E. Coronado, L.L. Zhao, G.C. Schatz, J. Phys. Chem. B 107 (2003) 668.
[35] C. Sönnichsen, T. Franzl, T. Wilk, G. von Plessen, J. Feldmann, New J. Phys. 93 (2002) 1.
[36] F. Stietz, F. Träger, Philos. Mag. B 79 (1999) 1281.
[37] J.J. Mock, M. Barbic, D.R. Smith, D.A. Schultz, S. Schultz, J. Chem. Phys. 116 (2002) 6755.
[38] P. Mulvaney, Langmuir 12 (1996) 788.
[39] A. Hilger, M. Tenfelde, U. Kreibig, Appl. Phys. B 73 (2001) 361.
[40] T. Jensen, L. Kelly, A. Lazarides, G.C. Schatz, J. Cluster Sci. 10 (1999) 295.
[41] U. Kreibig, L. Genzel, Surf. Sci. 156 (1985) 678.
[42] B.D. Cullity, in: Elements of X-Ray Diffraction, second ed., Addison–Wesley, Menlo Park, CA, 1978, p. 102.
[43] R. Seyedmonir, D.E. Strohmayer, G.L. Geoffroy, M.A. Vannice, Adsorpt. Sci. Technol. 1 (1984) 253.
[44] K.M. Kholyavenko, M.Y. Rubanic, N.A. Cheryukhiva, Kinet. Catal. 5 (1964) 437.
[45] J.F. Scholten, J.A. Konvalinka, F.W. Beeckman, J. Catal. 28 (1973) 209.
[46] R. Seyedmonir, D.E. Strohmayer, G.L. Geoffroy, M.A. Vannice, H.W. Young, J.W. Linowski, J. Catal. 87 (1984) 424.
[47] J.K. Plischke, M.A. Vannice, Appl. Catal. 42 (1988) 255.
[48] G. Kortüm, Reflectance Spectroscopy, Springer, Berlin, 1969.
[49] T. Wenzel, J. Bosbach, F. Stietz, F. Träger, Surf. Sci. 432 (1999) 257.
[50] E. Ruckenstein, S.H. Lee, J. Catal. 109 (1988) 100.
[51] M.V. Badani, M.A. Vannice, Appl. Catal. A 204 (2000) 129.
[52] D.E. Strohmayer, G.L. Geoffroy, M.A. Vannice, Appl. Catal. 7 (1983) 189.
[53] M. Todorova, X.X. Li, M.V. Ganduglia-Pirovano, C. Stampfl, K. Reuter, M. Scheffler, Phys. Rev. Lett. 89 (2002) 096103.
[54] W. Cai, H. Zhong, L. Zhang, J. Appl. Phys. 83 (1998) 1705.
[55] M. Akimoto, K. Ichikawa, E. Echigoya, J. Catal. 76 (1982) 333.
[56] M.A. Barteau, R.J. Madix, J. Am. Chem. Soc. 105 (1983) 344.
[57] J.T. Roberts, R.J. Madix, W.W. Crew, J. Catal. 141 (1993) 300.
[58] S.R. Seyedmonir, J.K. Plischke, M.A. Vannice, H.W. Young, J. Catal. 123 (1990) 534.
[59] A. Ayame, Y. Uchida, H. Ono, M. Miyamoto, T. Sato, H. Hayasaka, Appl. Catal. A 244 (2003) 59.
[60] M. Boudart, Adv. Catal. 20 (1969) 153.
[61] R. van Hardeveld, F. Hartog, Surf. Sci. 15 (1969) 189.
[62] J.K. Lee, X.E. Verykios, R. Pitchai, Appl. Catal. 50 (1989) 171.
[63] N. Bogdanchikova, F.C. Meunier, M. Avalos-Borja, J.P. Breen, A. Pestryakov, Appl. Catal. B 36 (2002) 287.
[64] V.I. Bukhtiyarov, A.I. Boronin, V.I. Savchenko, J. Catal. 150 (1994) 262.
[65] R.A. van Santen, H.P.C.E. Kuipers, Adv. Catal. 35 (1987) 265.
[66] C. Backx, J. Moolhuysen, P. Geenen, R.A. van Santen, J. Catal. 72 (1981) 364.
[67] C.J. Bertole, C.A. Mims, J. Catal. 188 (1999) 58.
[68] C. Stegelmann, P. Stoltze, J. Catal. 226 (2004) 129.
[69] V.B. Kazansky, V.A. Shvets, M.Y. Kon, V.V. Nikisha, B.N. Shelimov, in: J. Hightower (Ed.), Catalysis, North-Holland, Amsterdam, 1973, p. 1423.
[70] V.I. Bukhtiyarov, M. Hävecker, V.V. Kaichev, A. Knop-Gericke, R.W. Mayer, R. Schlögl, Phys. Rev. B 67 (2003) 235422.
[71] R.M. Lambert, F.J. Williams, R.L. Cropley, A. Palermo, J. Mol. Catal. A: Chem. 228 (2005) 27.